The Korean Journal of Ceramics, 4 [4] 345 - 351 (1998)

Thermal Shock Resistance of Al_2O_3- and Fe-Al_2TiO_5-based Castable Refractories

T. Liu*, B. A. Latella and P. Bendeich

Materials Division, ANSTO, PMB-1, Menai, NSW 2234, Australia

(Received September 23, 1998)

Thermal shock resistance of Al_2O_3- and Fe-Al_2TiO_5-based castable refractories was studied using a central heating technique. Ring type specimens, 10 mm thick and 20 and 100 mm inner and outer diameters, respectively, were rapidly heated on the internal surface of the centre hole using a high power electrical heating element. The temperature field was measured experimentally and modelled using finite element analysis (FEA). The thermal stress field was also modelled using FEA. A radial notch was introduced to the ring specimens to enable calculation of the thermal stress intensity factors (SIF). A special LVDT device was incorporated in the thermal shock tester to monitor crack mouth opening displacement (COD). The thermal shock fracture initiation and crack propagation behaviour of the castable refractories were ascertained using the COD measurements and the fracture mechanics analysis data.

Key words : Thermal shock, Castable refractory, Modelling frarture initiation, Crack propagation

I. Introduction

Ceramic materials and refractories have been used for at least as long as man has been civilised, and because of their superior chemical and physical characteristics, they have found applications in many industrial and laboratory processes which involve high temperatures. During high temperature service, however, these materials may be subjected to high heat fluxes and rapid temperature variations resulting in non-uniform temperature distributions within the materials and the occurrence of non-uniform thermal stress fields. The inherent brittleness of these materials combined with these thermal stresses can often lead to microstructural damage or catastrophic failure. Improvements in materials reliability under such thermal shock conditions is one of the key steps for the future progress in the application of ceramics and refractories as high performance structural or functional materials.[1,2]

The most widely accepted and employed thermal shock techniques used in the evaluation of thermal shock properties of ceramics and refractories are quench techniques, especially the water quenching technique. However, the quench techniques used differ widely between laboratories and involve problems with experimental methods and uncertainties in measurements. The technique is suitable for comparing materials but not for measuring an absolute value as a characteristic material property.[2] Because of drawbacks with quenching, it has been necessary to develop and standardise new and novel thermal shock testing techniques. Several heating techniques, such as central heating of a disk specimen using laser beam, electron beam, arc discharge and high-powered light etc., have been developed to overcome the disadvantages of quenching techniques.[4-8] These heating techniques permit the temperature distribution to be measured experimentally, whilst the stress distribution of the specimen with respect to its change with heating time can be calculated analytically or numerically. Furthermore, these heating methods make it possible to evaluate the thermal shock resistance parameters from the power used and heating time. Thus, analysis using fracture mechanics becomes feasible.

The purpose of the present work was to develop a central heating thermal shock tester and to investigate the thermal shock behaviour of three refractories. The temperature field was measured experimentally and also modelled using finite element analysis (FEA). The thermal stress field was also modelled using FEA. A radial notch was introduced into the ring specimens to enable the thermal stress intensity factors (SIF) to be calculated. A special LVDT device was incorporated into the thermal shock tester to monitor the crack mouth opening displacement (COD). The thermal shock fracture behaviour of the three refractories was characterised by combining the COD measurements with the fracture mechanics analysis.

II. Materials, Testing Technique and Finite Element Analysis

1. Materials Characterisation

The thermal shock behaviour of three refractories was studied: an Fe-Al_2TiO_5-castable, an Al_2O_3-based zero cement castable and a fused-cast Al_2O_3. The microstructure and phase compositions of these materials were examined using scanning electron microscopy (SEM) on polished surfaces and X-ray diffraction (XRD). Elemental analysis

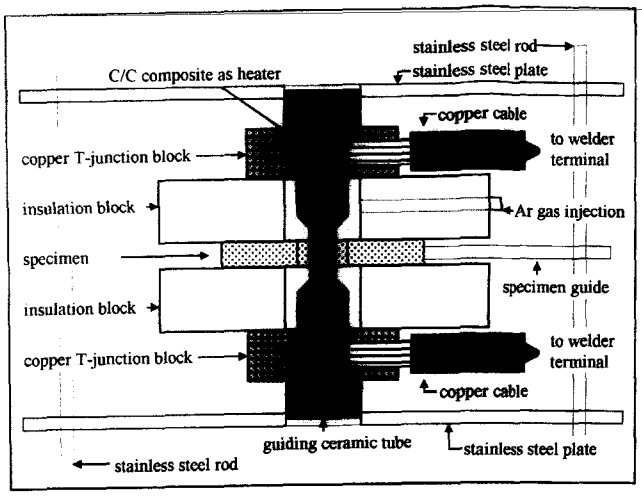

Fig. 1. Schematic of the central heating thermal shock tester.

of the phases was carried out by energy dispersive X-ray spectroscopy (EDS).

2. Thermal Shock Testing

The set-up of the thermal shock tester is shown schematically in Fig. 1. The test specimen, 20 mm and 100 mm inner and outer diameters, respectively and 10 mm thick, was sandwiched between two refractory insulation blocks. The internal surface of the centre hole of the ring specimen was heated with an electrical heating element. To ensure a high heating rate, an electrical current of up to 1000 A was applied to the heating element. The temperature field was measured using thermocouples and the data was logged with a Data-Taker (DT500) interfaced with a computer. To enable a fracture mechanics analysis of the thermal shock tests to be performed, a radial notch was cut in the specimen and the crack mouth opening displacement (COD) was monitored using a special LVDT device developed at ANSTO. Details about the special LVDT device were described previously.[10]

3. Finite Element Analysis

The FE analysis was carried out using the program NISAII (Engineering Mechanics Research Corporation, Troy, Michigan, USA). The analysis consisted of three parts: a) Transient thermal analysis, b) Static stress analysis and c) Fracture mechanics analysis. The transient thermal analysis was used to match the measured temperature profile of the specimen with time. This was accomplished by varying the internal wall heating rates until the model matched the measured results at the relevant radii. The subsequent static stress analysis used the results of the transient thermal analysis to establish a stress field for any given time step. Both axisymmetric (Fig. 2) and 2d plain stress (Fig. 3) models were used so that results could be crosschecked as far as possible with regard to mesh refinement. Temperature dependent elastic and thermal properties were used in

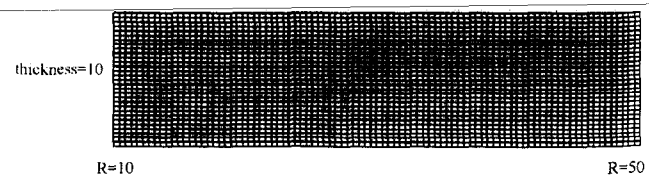

Fig. 2. Axisymmetric model of thermal shock test specimen.

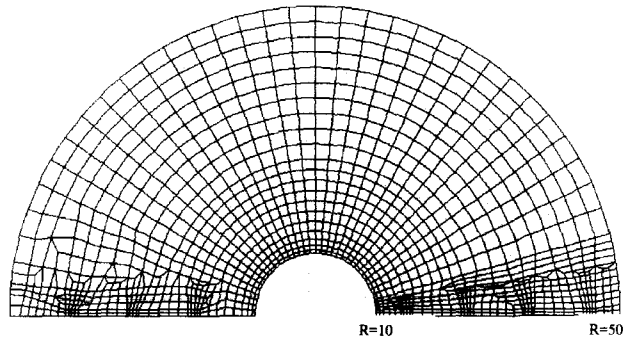

Fig. 3. 2d model of thermal shock test specimen.

the thermal, stress and fracture mechanics analysis. A half model was used in the 2d analysis due to the symmetry of the model and loading. Fracture mechanics analysis of the 2d-stress model, using the Virtual Crack Extension (VCE) method, resulted in the determination of stress intensity factors (SIF's) for various length cracks at varying time intervals. Removing the boundary displacement constraints along the appropriate section of symmetry interface had the effect of varying the length of the crack. In order to ensure an accurate solution at each crack tip, two levels of element refinement at the crack tip region were examined.

III. Results and Discussion

1. Microstructure and Phase Analysis

Fig. 4 shows backscattered electron images of the Fe-Al_2TiO_5-castable (ATC) refractory. The ATC consists of the Fe-Al_2TiO_5-ceramic aggregate and a cement as the binder (Fig. 4-a). The Fe-Al_2TiO_5-ceramic aggregate (Fig. 4-b) consists of four major phases, these include Al_2O_3 as the darkest phase, Al_2TiO_5 as the medium darkness, Fe-Al_2TiO_5 as a light grey and $CaTiO_3$ as a white phase. The black areas correspond to porosity in the material. As shown in Fig. 4-b, the Fe-Al_2TiO_5 phase is the most dominant phase in this material. Several minor constituents such as CaO, SiO_2 and P_2O_5 were also found as impurities in the major phases of Al_2O_3 and Al_2TiO_5. The ATC contains extensive microcracking and porosity both within and between the Fe-Al_2TiO_5-ceramic aggregates.

The microstructure of the zero cement castable (ZCC) is shown in Fig. 5. The ZCC was found to consist of Al_2O_3 as the predominant phase. The size of the Al_2O_3 phase varies from several microns to several millimetres. Minor

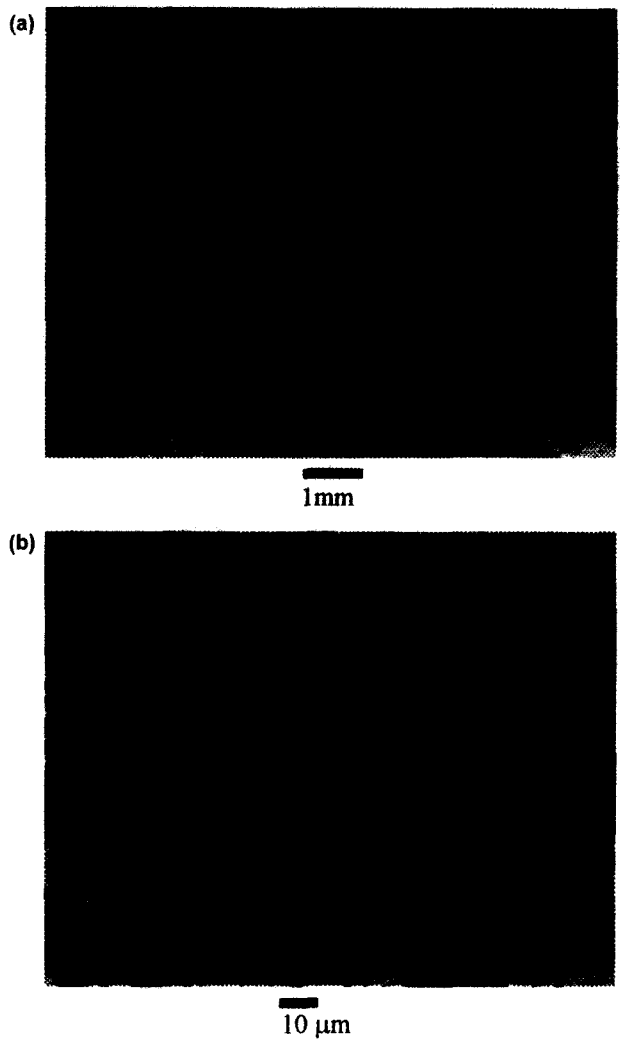

Fig. 4. SEM micrographs of the Fe-Al_2TiO_5 castable (ATC) showing (a) overview (low magnification) and (b) Fe-AT ceramic aggregate (high magnification).

elements observed in the Al_2O_3 phase were Fe, Si, Ca. The material was found to contain extensive porosity as

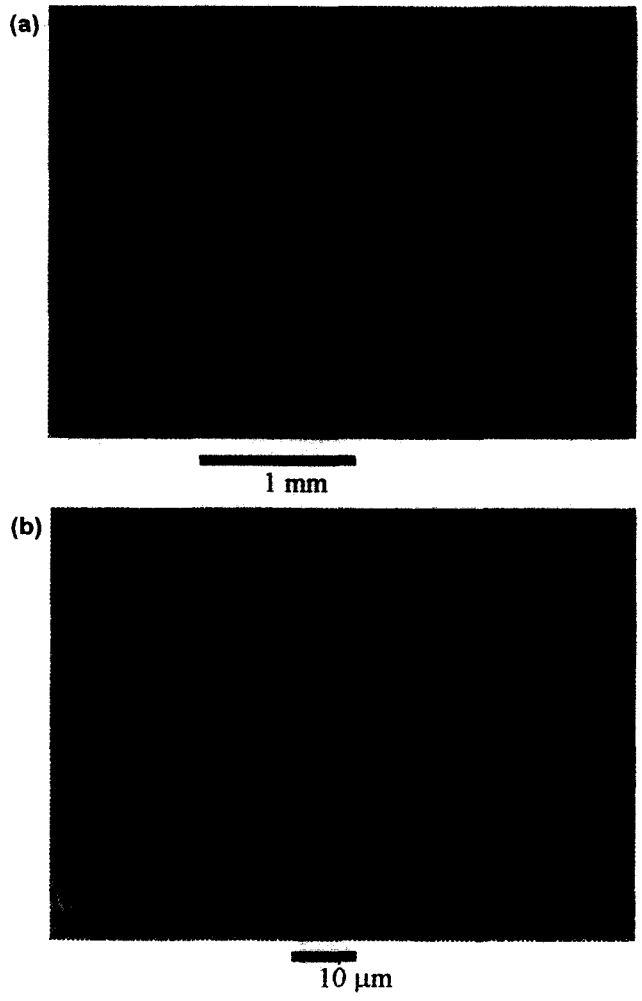

Fig. 5. SEM micrographs of the alumina zero cement castable (ZCC) showing (a) overview (low magnification) and (b) fine-

shown in Fig. 5-b.

The fused-cast Al_2O_3 refractory shown in Fig. 6 consists of two major Al_2O_3 phases, α-Al_2O_3 and β-Al_2O_3. No impurities were detected in the matrix of α-Al_2O_3, whilst Na and Ca were observed in β-Al_2O_3 grains.

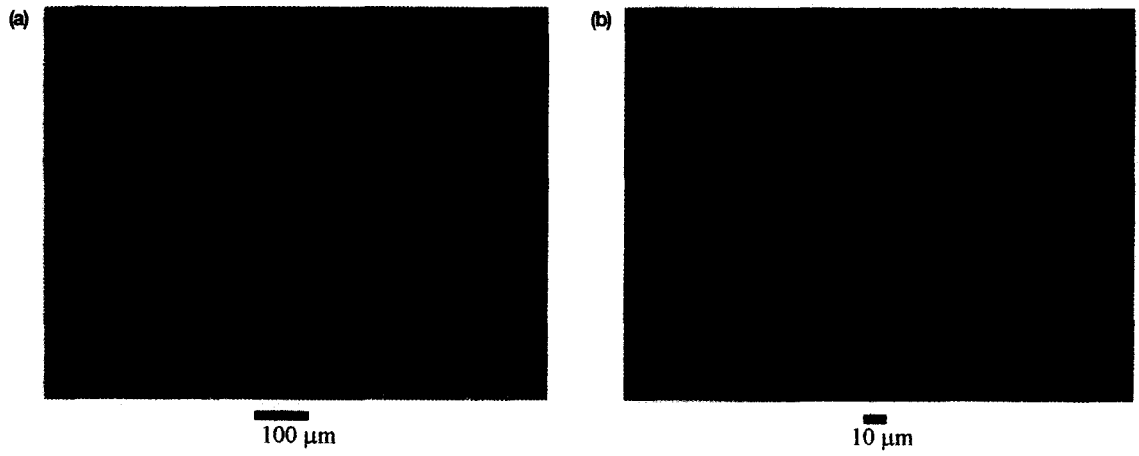

Fig. 6. SEM micrographs of the fused-cast Al_2O_3 showing (a) overview (low magnification) and (b) α- and β-Al_2O_3 (high magnification).

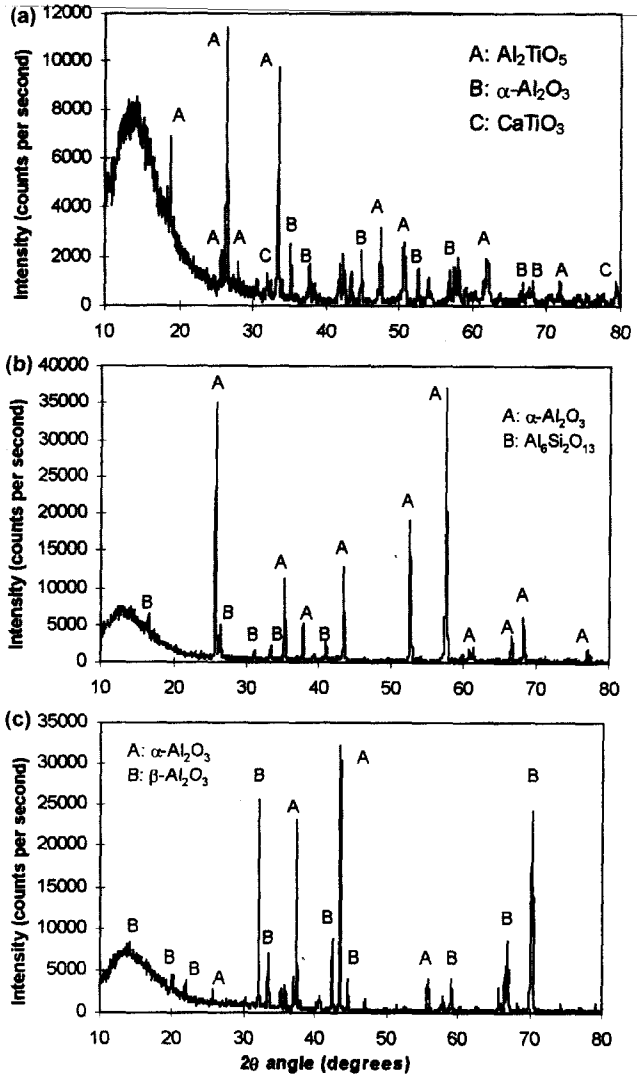

Fig. 7. XRD spectra of (a) ATC showing the presence of Al_2TiO_5 (major phase) and Al_2O_3 and $CaTiO_3$ (minor phases), (b) ZCC showing Al_2O_3 and mullite as the major and minor phases, respectively and (c) fused-cast alumina showing the presence of both α- and β-Al_2O_3.

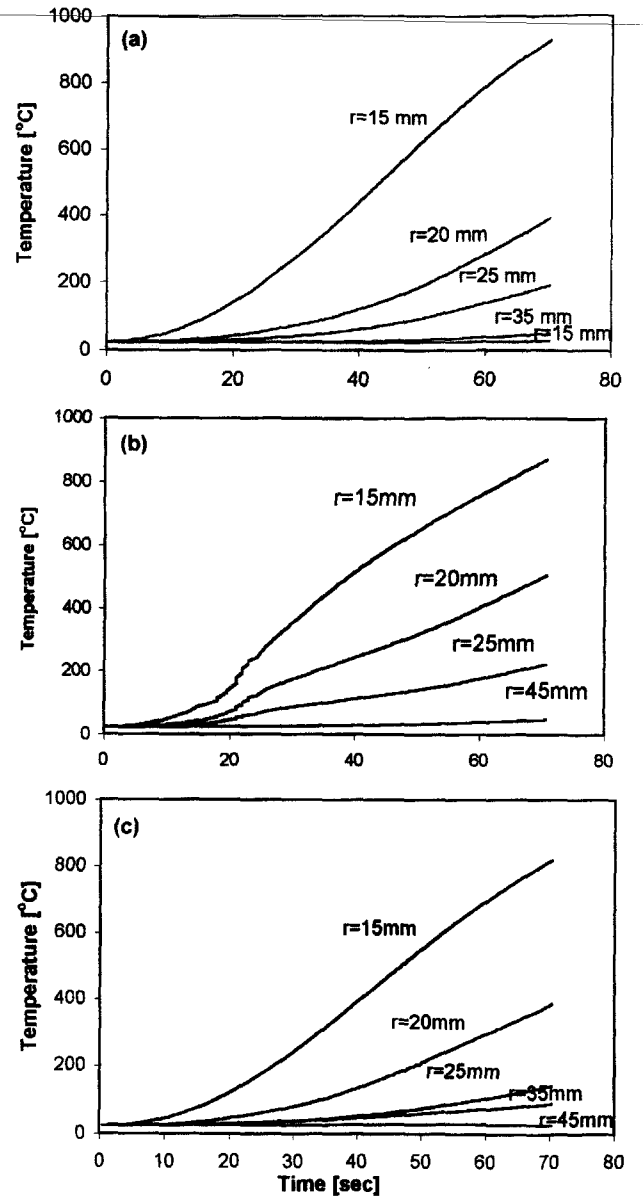

Fig. 8. Measured temperature-time curves of (a) fused-cast Al_2O_3, (b) ZCC and (c) ATC at radii indicated.

Fig. 7 shows the XRD spectra of the three materials examined. For the ATC, the presence of Al_2TiO_5 (as the two major peaks) was easily determined. Moreover, other phases, such as Al_2O_3 and $CaTiO_3$, were also readily identified by search match analysis. For the ZCC, the major phase found was Al_2O_3 (corundum) and a small amount of mullite phase was detected. For the fused-cast Al_2O_3, the XRD examination (Fig. 7-c) showed the presence of both α- and β-Al_2O_3.

2. *Thermal Shock Test Results*

Fig. 8 shows the experimentally measured temperature-time profiles of the three materials tested. From the measured temperatures at a radius of r=15 mm three types of heating rate were calculated: a) the average heating rate (=highest temperature/time required); b) the maximum heating rate at a point of differentiation (dT/dt); and c) maximum heating rate by linear regression. As shown in Table 1, the heating rate of the ATC is the highest, whilst that of the ZCC is lowest. The difference in the heating rate is caused mainly by the difference in the thermal conductivity of the materials.

Fig. 9 shows the temperature gradient of the three materials tested. Due to the difference in the heating rates a higher temperature gradient was observed in the ZCC, while the temperature gradient was lowest for the ATC.

Fig. 10 shows the COD versus time curves for the three materials tested. The AT-castable (ATC) showed no significant COD changes; that is, no discernible thermal expansion and crack propagation was observed. This

Table 1. Heating Rates ar r=15 mm for the three Materials Tested

Materials	ATC	Fused-cast alumina	ZCC
Average heating rate [°C/sec]	13.2	10.6	9.6
Maximum differential heating rate [°C/sec]	21.4	17.4	14.1
Maximum linear heating rate [°C/sec]	14.2	11.8	10.8

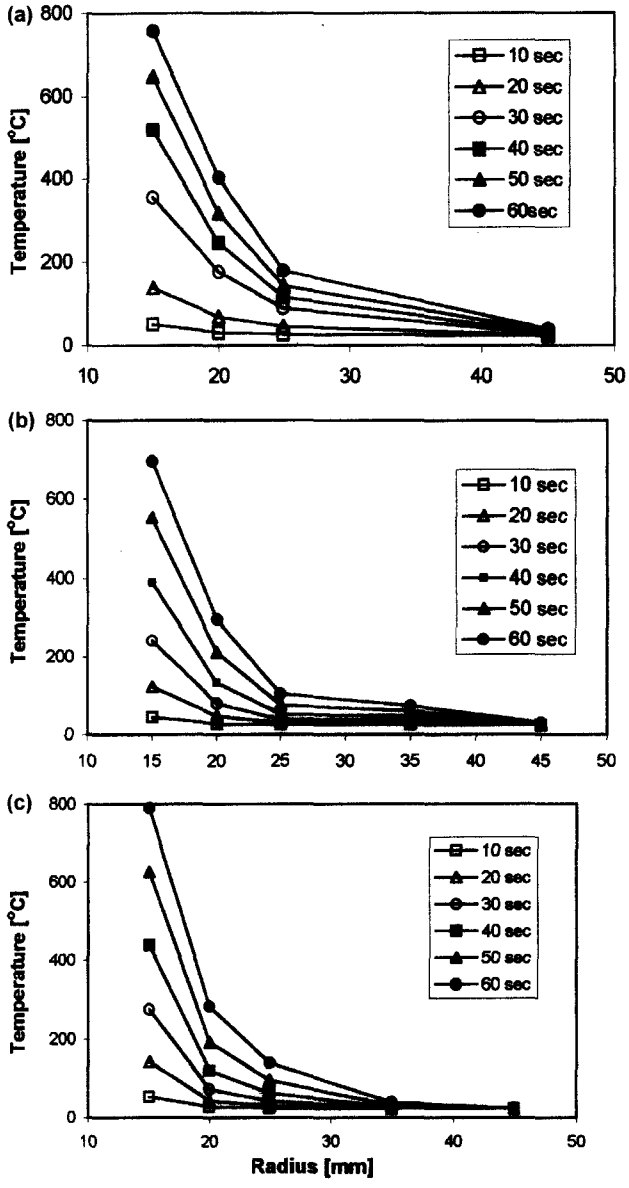

Fig. 9. Measured temperature gradient of (a) fused-cast Al_2O_3, (b) ZCC and (c) ATC at times indicated.

agrees well with the fact that the thermal expansion coefficient of ATC is almost zero.[9] It therefore shows excellent thermal shock resistance. For the fused-cast Al_2O_3 specimen, a small COD jump of about 23 μm occurred at 18 seconds. For this material, it can be concluded that the value of COD jump is small while the t_C was found to be 18 seconds. For the zero-cement castable Al_2O_3 (ZCC), the COD jump determined from the thermal

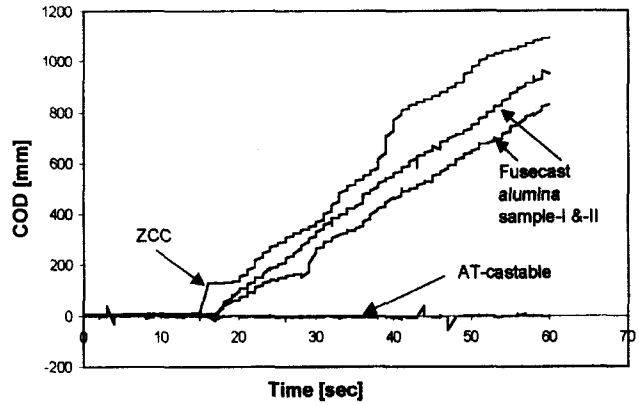

Fig. 10. Measured CMOD-time curves of the ATC, ZCC and fused-cast alumina.

Table 2. COD jump and Time for Thermal Shock Fracture

	CMOD jump (microns)	Time, t_C (seconds)
ATC	None	None
Fused-cast alumina	23	18
ZCC	116	15

shock test was 116 μm. The time for fracture initiation, t_C, was found to be 15 seconds.

The value of $1t_C$ can be used as a measure of the thermal shock fracture initiation resistance of materials. The longer the time, the greater is the fracture initiation resistance. The COD jump represents the crack propagation resistance of a material. The larger the COD jump, the lower the crack propagation resistance. Detailed analysis of $1t_C$ and COD jump was described in [10]. Table 2 summarises the results of the thermal shock tests, where the time for fracture initiation and the COD jump are listed. From Table 2 it may be concluded that the relative thermal shock resistance of the three refractories is:

ATC>>fused-cast alumina>ZZC

3. Finite Element and Fracture Mechanics Analysis

Fig. 11 shows the temperature-time profiles of the fused-cast alumina, where the thick lines represent the temperature measured experimentally using thermocouples and the thin lines represent the modelled temperature.

Based on the temperature profiles as shown in Fig. 11, the thermal stress was modelled using finite element analysis. Fig. 12 shows the results of the hoop stress for an unnotched disk. A clear transition from compressive to tensile stress is observed with increasing radius. The

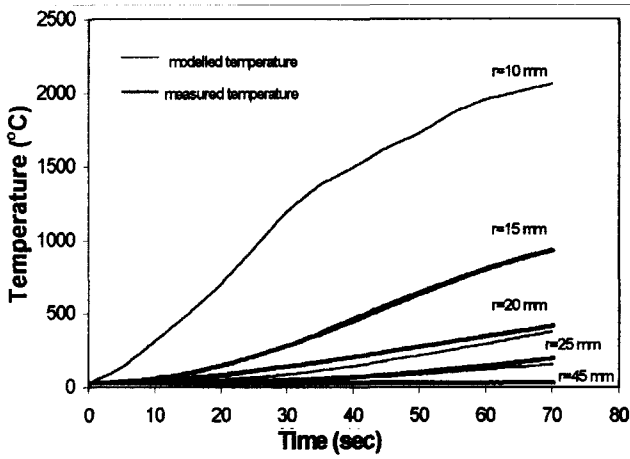

Fig. 11. Measured (thick lines) and modelled (thin lines) temperature-time curves for the fused-cast alumina at radii indicated.

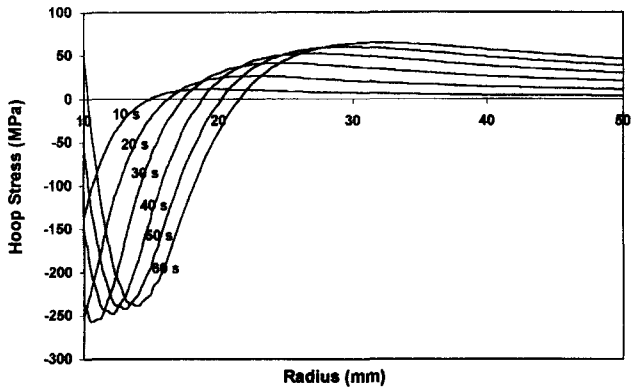

Fig. 12. Modelled hoop stress distribution for an unnotched disk of the fused-cast alumina at times indicated.

magnitude of the compression and tensile stress increases with time. It is interesting to note that the hoop stress goes through a minimum. The radius, at which the minimum stress occurs, is shifted in the direction of larger radius with increasing time. This is caused by the fact that the Young's modulus of the fused-cast alumina decreases with increasing temperature. From 30 seconds onwards, the temperature at the internal surface is so high, that the material starts to yield or deform plastically. Consequently the compressive stress is relaxed. In fact, with further increased heating time, tensile stress will appear on the internal surface of the specimen.

Fig. 13 shows the stress intensity factor as a function of crack length. The stress intensity factor increases dramatically with increasing time and crack length. From this figure the thermal shock fracture toughness can be analysed. For example, if the starting notch length is 10 mm and the onset of the thermal shock fracture initiation is 20 seconds, then the point "E" in Fig. 13 represents the thermal shock fracture toughness, $K_{Ic,ts}$. For the fused-cast alumina, the time for thermal shock fracture initiation was 15 seconds. The thermal shock

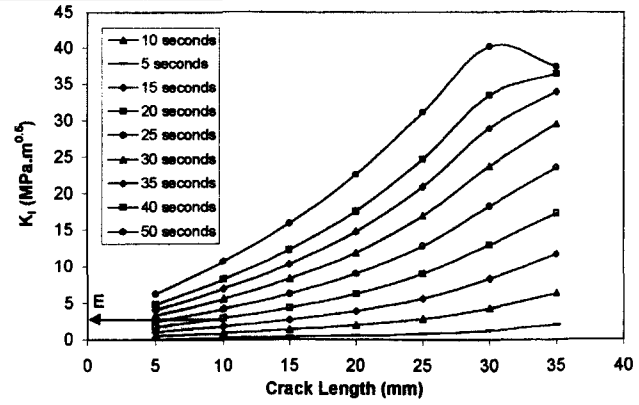

Fig. 13. Normalised stress intensity factor as a function of crack length.

fracture toughness derived from Fig. 13 is about 2.1 MPa.m$^{0.5}$.

IV. Conclusions

A thermal shock technique has been developed which is capable of assessing thermal shock resistance of refractories with defined fields of temperature, stress and stress intensity. Using this technique the thermal shock resistance of three refractory materials was tested. The following conclusions can be drawn from this work:

(1) The Fe-Al_2TiO_5-castable refractory exhibits excellent thermal shock resistance due to its near zero coefficient of thermal expansion. Despite the severe thermal shock condition in the thermal shock test, no cracking/fracture was observed in this material.

(2) Thermal shock cracking was observed in the zero cement castable and the fused-cast alumina refractories. The fused-cast alumina refractory exhibits a longer time for thermal shock fracture, t_c, and smaller COD jump at t_c. which indicates that the thermal shock resistance of the fused-cast alumina is higher than the zero cement castable alumina (ZCC).

(3) Thermal shock fracture toughness, $K_{Ic,ts}$, can be determined by experimentally measuring the COD versus time curves and modelling the field of thermal stress and stress intensity factor using finite element analysis. The $K_{Ic,ts}$ of the fused-cast alumina was determined as 2.1 MPa.m$^{0.5}$.

Acknowledgments

The authors would like to thank Y. Muroi for assistance with performing the thermal shock tests. Technical support provided by M. Bloom, S. Leung, K. McKay and F. Van Luyt is also gratefully acknowledged.

References

1. D. P. H. Hasselman, "Thermal Stress Resistance Para-

meters for Brittle Refractory Ceramics: A Compendium," *Am. Ceram. Soc. Bull.*, **49**(12), 1033-37 (1970).
2. W. E. Pompe, "Thermal Shock Behaviour of Ceramic Materials-Modelling and Measurement," pp. 3-14 in *Thermal Shock and Thermal Fatigue Behaviour of Advanced Ceramics*. Edited by G. A. Schneider and G. Petzow. Kluwer Academic Publishers, Netherlands, 1993.
3. W. D. Kingery, "Factors Affecting Thermal Stress Resistance of Ceramic Materials," *J. Am. Ceram. Soc.*, **38**(1), 3-15 (1955).
4. G. Kirchhoff, "Thermal Shock Fracture by Laser Irradiation," pp. 245-251 in "Thermal Shock and Thermal Fatigue Behaviour of Advanced Ceramics". Edited by G. A. Schneider and G. Petzow. Kluwer Academic Publishers, Netherlands, 1993.
5. C. Schubert, H. A. Bahr and H. J. Weiss, "Crack Propagation and Thermal Shock Damage in Graphite Disks Heated by Moving Electron Beam," *Acta Metall.*, **24**(1), 21-28 (1986).
6. S. Sato, Y Imamura, A. Kurumada, K. Kawamata, R. Ishida and H. Awaji, "Evaluations of the Thermal Shock Resistance and Fracture Toughness of Graphite and C/C Composites by Arc Discharge Heating," pp. 253-268 in "Thermal Shock and Thermal Fatigue Behaviour of Advanced Ceramics". Edited by G. A. Schneider and G. Petzow. Kluwer Academic Publishers, Netherlands, 1993.
7. G. A. Schneider and G. Petzow, "Thermal Shock Testing of Ceramics-A New Testing Method," *J. Am. Ceram. Soc.*, **74**(1), 98-102 (1991).
8. G. A. Gogotsi, V. I. Galenko, V. P. Zavada and M. V. Swain, "Influence of Heating Rate on the thermal Strain Induced Fracture of Mg-PSZ Sample," pp. 293-305 in "Thermal Shock and Thermal Fatigue Behaviour of Advanced Ceramics". Edited by G. A. Schneider and G. Petzow. Kluwer Academic Publishers, Netherlands, 1993.
9. D. Perera, "Fabrication of Aluminium Titanate As A Castable," ANSTO Technical Report, April 1997.
10. T. Liu, P. S. Cook, C. P. Hughes and B. J. Mason, "Thermal Shock Crack Initiation and Propagation Behaviour of Carbon Anodes," *Light Metals* (1995), pp. 733-740.